Research Article

Green synthesis and characterization of zinc oxide nanoparticles using *Eucalyptus globulus* Labill. leaf extract and zinc nitrate hexahydrate salt

Azeez Abdullah Barzinjy[1,2] · **Himdad Hamad Azeez**[1]

Received: 4 February 2020 / Accepted: 22 April 2020 / Published online: 30 April 2020

Abstract
This study consists of a reliable process for synthesizing ZnO NPs by green method. Here, *Eucalyptus globulus* Labill. leaf extract is utilized as an efficient chelating and capping agent for synthesizing ZnO NPs from zinc nitrate hexahydrate salt. The plant ingredients, structure, morphology, thermal behavior, chemical composition and optical properties of ZnO nanoparticles were investigated using several characterization techniques, namely XRD, FE-SEM, EDX, BET, Zeta potential, DLS, differential scanning calorimetry (DSC) analysis, FT-IR analysis and UV–Vis spectroscopy. The UV–Vis and FTIR analysis of *Eucalyptus globulus* leaf extract verified that this extract is a promising candidate for biosynthesizing ZnO NPs. The XRD spectrum, DLS and the SEM images confirmed the crystallinity and the spherical-shape of the ZnO NPs with an average size between 27 and 35 nm. The band-gap of the ZnO were measured to be around 2.67 eV. Zeta potential and BET analysis showed that, the biosynthesized ZnO NPs possess good stability and the their specific surface area is 23.481 m^2/g. DSC analysis exhibits two endothermic peaks related to the water evaporation absorbed by the NPs and modification of zinc complex to zinc hydroxide, with a single exothermic peak related to the crystallization of ZnO NPs and degradation of organic materials.

Keywords Green synthesis method of NPs · ZnO NPs · *Eucalyptus globulus* · Zinc nitrate hexahydrate · Biosynthesis

1 Introduction

Nanoparticles display novel characteristics which vary considerably from those shown by their bulk material equivalents due to their extremely tiny sizes, i.e. order of 10^{-9} m. Their tiny dimensions provide them extraordinary surface-to-volume ratios which permit them to confine electron motions inside boundaries associated with improving the optical properties. This makes them particularly desirable in various application areas such as medicine [1], drug delivery [2], water purification [3], agriculture [4], food [5], solar cells [6], cosmetics [7], textiles [8] and electronics [9].

Metals and metal oxides nanomaterial exhibit vital physicochemical properties which include higher conductivity, catalytic activity; unusual optical properties and pyro-mechanical properties. They also have antimicrobial activity against pathogenic microorganisms [10–13]. Concerning the biological activity of nanoparticles, it has been shown that silver (Ag NPs) and zinc oxide (ZnO NPs) have an inhibitory effect on the growth of bacterial and fungal strains, when used in concentrations comparable to those used in antibiotics to treat infectious diseases [14, 15].

It has been proven that metal nanoparticles, despite offering antimicrobial activity, could exhibit cytotoxic effects on healthy and carcinogenic cell lines, depending on the concentration used [16, 17]. In addition, it has been indicated that the stability of nanoparticles is

✉ Azeez Abdullah Barzinjy, azeez.azeez@su.edu.krd | [1]Department of Physics, College of Education, Salahaddin University-Erbil, Erbil, Kurdistan Region, Iraq. [2]Department of Physics Education, Faculty of Education, Tishk International University, Erbil, Kurdistan Region, Iraq.

endangered in physiological conditions since the presence of biological compounds such as enzymes can delay the effective action of nanoparticles at the site of infection.

Nowadays, various physical, chemical, biological and hybrid approaches are applied effectively in the production of different types of inorganic NPs, nevertheless they are pricey and need the usage of damaging chemical substances. Therefore, our environment is suffering from harm and an enormous quantity of unwanted materials [18]. For the time being, we need to discover the paradoxes that may exist in nature for alternative plans. In this manner, we will be able to deal with environmentally friendly and repairable materials, and completely away from using toxic materials. These novel spotless skills can extremely decrease ecological pollution and decline the danger to human healthiness as a result of utilizing harmful chemicals and solvents [19]. On the other hand, producing nanoparticles from physical and chemical approaches, with various dimensions and shapes, require stabilizing agents since in most cases they are unsteady [20].

Biosynthesized NPs from plant extracts are, usually, prepared from biological part of plants. Plant parts, for instance leaf, root, stem and seed, are widely utilized for synthesizing metal-based NPs. Moreover, plant extracts contain bioactive polyphenols, alkaloids, proteins, sugars, phenolic acids, terpenoids, etc., they play a significant role in reducing the metallic ions and later stabilizing them [21].

In order to solve the difficulties involved in the use of nanoparticles as antimicrobial agents, encapsulation of metal nanoparticles has been proposed as a strategy that would reduce the possible cytotoxic effect, improve stability and increase bioavailability. Thus, the degradation would be avoided, and therefore the circulation time would be increased allowing a controlled release of the active agent. Figure 1 displays the grouping of dissimilar NP production methods.

The Biosynthesis of plant mediated nanoparticles can be classified into three phases: reduction phase, growth phase and stabilization phase [22]. The reduction phase is the most important phase wherein the metal ions are recovered from their salt forerunners over the interaction of plant metabolites; biomolecules that possess reduction capacities. The metal ions are transferred from their mono/divalent oxidation statuses to zero valent statuses, then nucleation of the reduced metal atoms occurs [23]. Then the growth phase comes wherein the separated metal atoms merge to form metal nanoparticles, however, additional biological reduction of metal ions happens. The growth phase increases in enhanced thermodynamic steadiness of nanoparticles while the widespread nucleation might cause aggregation of produced nanoparticles, changing their morphologies. The final phase in biosynthesis of nanoparticles is the stabilization phase. The nanoparticles eventually get their most intensely favorable and steady morphology when capped through plant metabolites. The effective mechanism of green synthesis using plants is shown in Fig. 2.

In fact, several characteristics of the solution combination such as; the concentration of metal salt, plant extract concentration, pH of the reaction solution, etc., and extra reaction circumstances such as reaction period and temperature have wide-ranging effects on the size, shape and quality of the biosynthesized nanoparticles [24, 25].

This study purposely focused on zinc oxide (ZnO) since ZnO is one of the most in-depth research semiconductor type metal oxides [26]. Among the semiconductor materials, ZnO possesses a wide band-gap of about 3.37 eV as well as an exciton binding energy of 60 meV [27] and Wurtzite structure (Fig. 3). Besides the semiconductor characteristic,

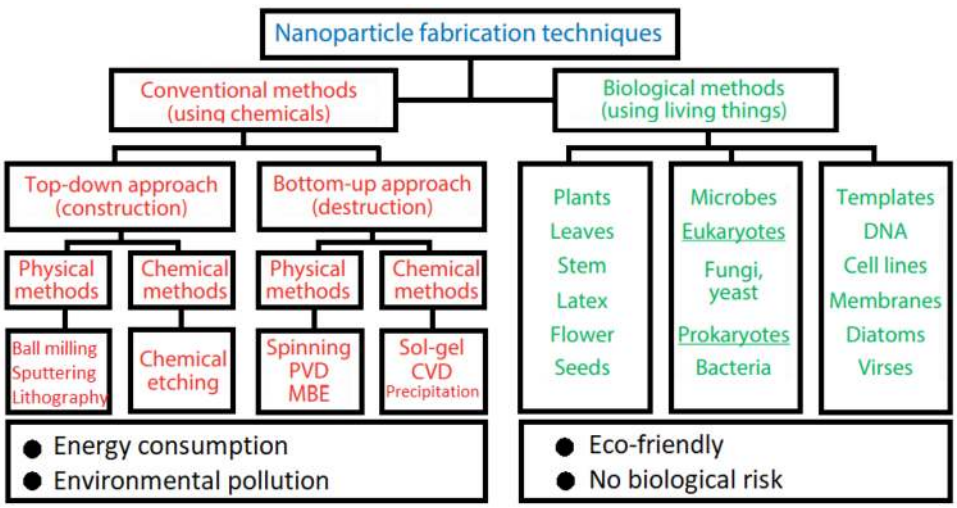

Fig. 1 Grouping of dissimilar nanoparticles production procedures

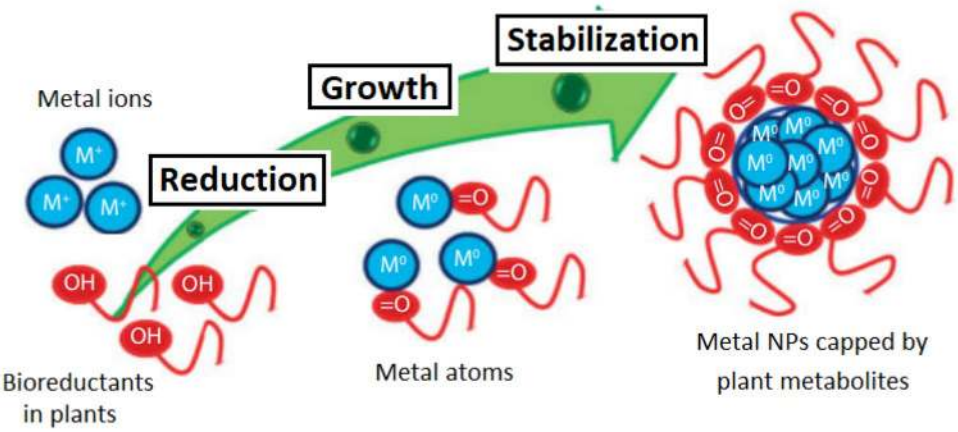

Fig. 2 Biosynthesis mechanism for producing metal NPs

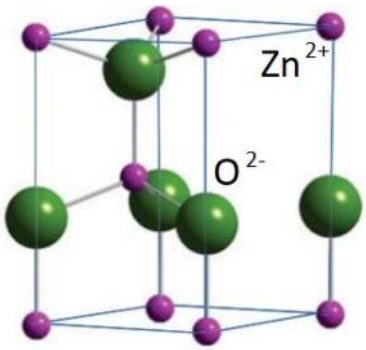

Fig. 3 Wurtzite structure of zinc oxide (ZnO)

ZnO possesses fascinating piezoelectric [28], oxidizing, [29] antibacterial, and photo-catalytic characteristics [30].

As a photo-catalyst, ZnO and its nano-composites exhibit outstanding aptitude in the direction of the degradation of organic pollutants in water under the ultra-violet radiation [31]. Thus, the photo-catalytic action of ZnO is achieved when the particles are in the nano-size range (1–100 nm) contrary to the macroscopic or bulk size. In addition, ZnO NPs showed a significant role in solar energy adaptation equipment due to its effective photo activity, high steadiness, cheap price and comparative harmlessness toward human beings and the surroundings [32].

The significance of this study is ZnO NPs has been synthesized through an easy method that avoids toxic chemicals and difficult experimental processes. Then the biosynthesized ZnO NPs from *Eucalyptus globulus* leaf extract can be utilized for many applications such as; photocatalytic activity, i.e. removing the organic pollutants in water, solar cell, Medical and Cosmetic applications.

2 Materials and methods

Zinc nitrate hexahydrate, Zn $(NO_3)_2{\cdot}6H_2O$ Molecular weight 297.48 g/mol and purity > 98.0%), sodium hydroxide pellets, and NaOH Molecular weight 40 g/mol, were purchased from Sigma-Aldrich and utilized as received-commercially with unpolluted specialized status. Fisher Scientific 11-600-49sh Isotemp Analog Hot Plate Stirrer was utilized as the heating source for the production of ZnO NPs. During the course of the ZnO NPs synthesis period, the hot plate was heated and the hot plate surface temperature was chosen to be around 80 °C. X-ray diffraction (XRD) measurements were carried out using a PAN analytical X' Pert PRO (Cu Kα = 1.5406 Å). The scanning rate was 1°/min in the 2θ range from 20° to 80°. UV–Vis spectral analysis was recorded on a double-beam spectrophotometer (Super Aquarius spectrophotometer) to ensure the formation of ZnO NPs. Morphology and particle dispersion were investigated by field emission scanning electron microscopy (FESEM) (Quanta 4500). The chemical composition of the prepared nanostructures was measured by EDX (Energy Dispersive X-ray Spectroscopy) performed in FESEM. FT-IR analysis was carried out using a Perkin Elmer. FTIR spectrophotometer with a resolution of 4 cm^{-1} was used for investigation of the functional groups in the leaf extract and the NPs. The size of ZnO NPs were characterized by by dynamic light scattering. The particle size was computed utilizing a Malvern Zetasizer 3000HSA (Malvern, Worcs., UK) equipped with a 10-mW He–Ne laser (633 nm) and functioning at an angle of 90° and a temperature of 20 °C. T. Differential scanning colorimetery (DSC) type (TA Instruments USA, DSC Q10) in the range 50–600 °C was utilized for the DSC curve. Thermogravimetric analysis (TGA) was performed using Perkin-Elmer-Pyris1 analyzer (USA). The specific surface area of ZnO NPs were determined by nitrogen absorption BET method which was conducted on a Micromeritics ASAP 200 instrument

at the Ulster University in the UK. Adsorption data for nitrogen at the liquid nitrogen gas temperature, 77 K, were utilized.

2.1 Preparation of plant extract

Eucalyptus globulus Labill is an aromatic tree belong to Myrtle family. Normally reaches a height of 45.7–54.9 m and a diameter of 1.2–2.1 m [33]. In this study, *Eucalyptus globulus* Labill. was collected in Sami Abdulrahman Park (Latitude 36°11′28.9″N and Longitude 43°58′42.3″E) in Erbil city, Iraqi Kurdistan Region in spring season (April 2019). Fresh leaves of *Eucalyptus globulus* Labill. were washed several times with Distilled water, and then dehydrated to remove the remaining dust particles and moisture. Later, the leaves were converted to small pieces by cutting them. About 20 g of the small pieces of leaves and 5 mL of distilled water were put into a mortar and pastel and crushed into paste. 6 g of this paste was mixed with 100 mL of distilled water in a beaker, after that, 2 Mole of NaOH solution was added dropwise to regulate the pH of the mixture, observed by a pH meter, to pH 8. The pH was not selected arbitrarily, since according to the literatures, in general, smaller sized NPs produced at higher pH [34].

Then the mixture was stirred almost continuously for 1 h producing a cloudy precipitous of zinc hydroxide, Zn $(OH)_2$, which was then centrifuged at 5000 rpm for 1 h and dried in an oven set to 60 °C. After that the mixture cooled to room temperature (Fig. 4).

2.2 Synthesis of zinc oxide nanoparticles

ZnO NPs were prepared utilizing green synthesis method by means of *Eucalyptus globulus* Labill. extract. After preparation of the plant extract as described previously, 30 mL of this extract was put into a beaker and heated gradually. When the temperature reached 60 °C, 3 g of zinc nitrate hexahydrate were added to this extract. After that the mixture was continuously stirred, maintaining the temperature at 60 °C, until the mixture converted into a yellowish paste after 1 h. It is obvious that, the temperature of reaction played important role in producing NPs, the optimal yield of NPs were achieved at 60 °C. Afterward the paste was blazed in a furnace at 400 °C for about 2 h then the residual was washed by ethanol and distilled water several times. The powder was then heated at 100 °C to dry. Then zinc oxide nanoparticles were obtained and they were ready for characterization. The middle of Fig. 4 shows the procedure of synthesizing zinc oxide nanoparticles using *Eucalyptus globulus* Labill. leaves extract and zinc nitrate hexahydrate as a precursor.

The mechanism and the responsible biomolecules for the nanoparticle's formation via plant extracts have not yet been entirely documented [35]. The plausible mechanism

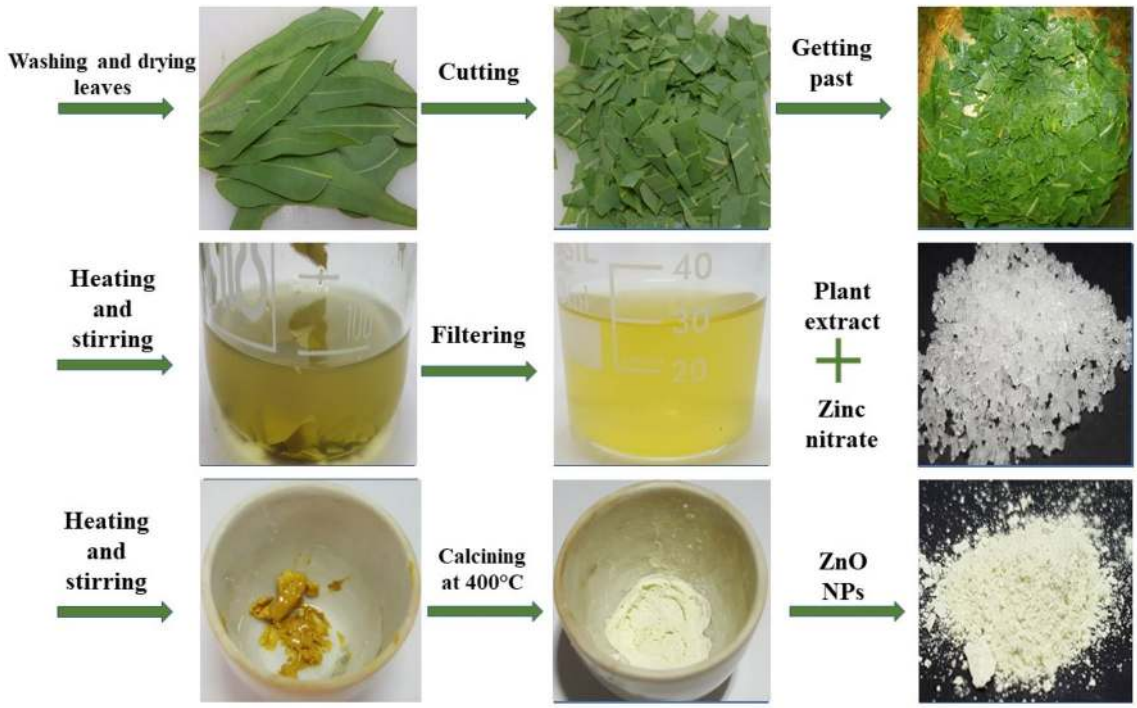

Fig. 4 Schematic representation of ZnO NPs synthesis using the leaf extract of *Eucalyptus globulus* Labill. and zinc nitrate hexahydrate

of ZnO NPs formation, using *Eucalyptus globulus* leaf extracts, is described as the following.

$$nZn^{2+} + 2Ar - (OH)_n \rightarrow nZn^0 + 2nAr = O + 2nH^+ \quad (1)$$

$$2(x+1)Zn^0 + 2Ar = O + yO_2 \rightarrow 2\left(Zn^0 - Zn_xO_y - Ar = O\right) \quad (2)$$

The biomolecules such as Tannins and flavonoids ($Ar–(OH)_n$) of *Eucalyptus globulus* leaf extracts, responsible for formation ZnO NPs, could lose their electron for the efficient reduction of Zn^{2+} ions to Zn^0. This might cause the Zn^0-phenolate complex by chelating effect causing nucleation and growth of NPs at 60 °C. This complex undergoes direct decomposition at higher temperature of 100 °C in air and lead to Zn NPs. Thus, the natural phenolic compounds had favorable effects on ZnO NPs synthesis.

3 Results and discussion

3.1 Characterization of *Eucalyptus globulus* Labill. leaf extract

3.1.1 UV–Vis analysis

Nowadays, in order to control the size and morphology of nanoparticles, investigators are using the individual plant phytochemicals for biosynthesizing nanoparticles. The phytochemicals presence in the plant extract reduces metal ion to metal nanoparticles. Therefore, plant extract, at the same time, acts as a reducing and stabilizing agent. UV–Vis spectroscopy monitors this reaction progress. Spectra of UV–Vis spectroscopy displayed a peak absorption correlated with the surface plasmon resonance, SPR, and collects conduction band electrons oscillations in reacting with electromagnetic waves, representing metal ion reduction and nanoparticle formation. *Eucalyptus globulus* Extract (Fig. 5a) possesses only one peak, namely 257 nm. Tannins and flavonoids are considered the major phytochemical component of *Eucalyptus globulus* extract (Fig. 5b) which are considered as possible bio-reducing and stabilizing agents, due to the availability of OH groups, for nanoparticles synthesis [35]. These phytochemicals, being antioxidant and free from toxic chemicals, are extremely capable of reducing metal ions and stabilizing them in nanoscale dimension. They can also provide nanoparticles of different shapes and dimensions [36].

The OH groups form a complex of $Zn(OH)_2$ with the zinc ions. The mechanisms of the phase transformation from $Zn(OH)_2$ to ZnO takes place in three ways, i.e. dissolutio–reprecipitation, in situ crystallization and solid–solid phase transformation. The loss of water from the lattice throughout the solid–solid phase transformation has also been suggested by Wang et al. [37].

We deduced that the maximum peaks, at 257 nm, in Fig. 5a might be associated with Tannin and flavonoid existing in *Eucalyptus globulus* leaf extract. According to the literature the absorption in the range 250–270 nm regions perhaps referring to the electronic transitions of benzene and its products, which might comprise numerous aromatic compounds like phenolics which is reach in O–H groups [38]. Makarov et al. [39] claims that flavonoids, in general, through their OH group switched from the enol-mold to the keto-mold [40], donating a responsive hydrogen atom which reduces the metallic ion into nanoparticles. Among those functional organic-molecules the

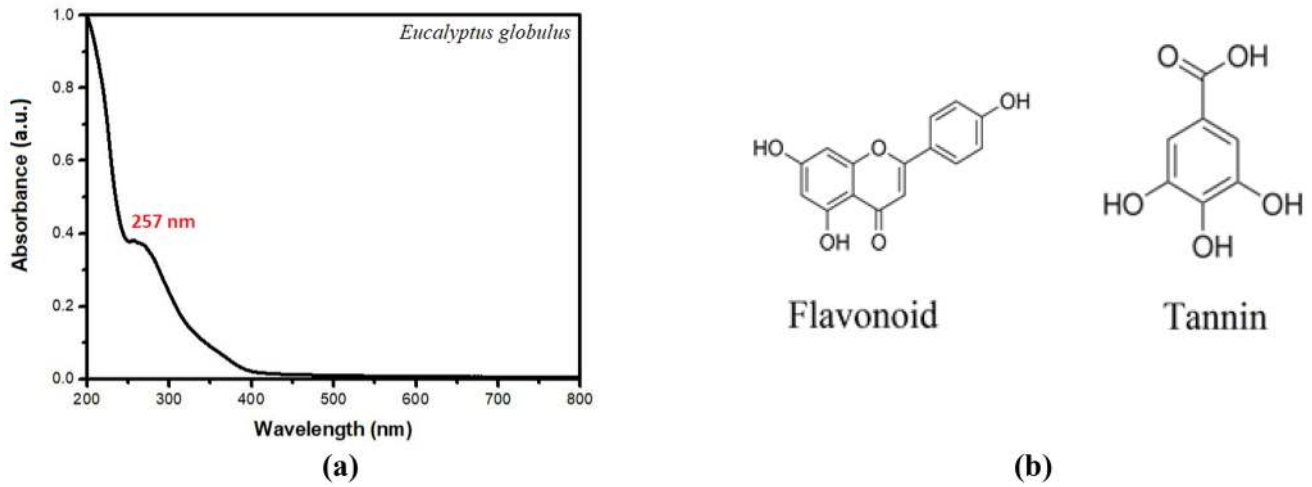

Fig. 5 **a** UV–Vis spectra of *Eucalyptus globulus* leaf extract, and **b** major phytochemical component of *Eucalyptus globulus* extract

flavonoids combinations existing in the extract more likely had great empathies on the metals [41], that reduced Zn^{2+} to Zn^0 [42]. Throughout air-drying, the produced Zn^0 were oxidized to produce ZnO NPs [43].

3.1.2 FT-IR analysis

The Fourier transform infrared, FTIR, spectra of the plant extract and ZnO NPs were examined to figure out if the functional groups related to these reductive biomolecules exists and specifying the functional groups that contributed to reduction of the ZnO into nanoparticles. *Eucalyptus globulus* Leaf extract (Fig. 6) possesses numerous bonds. The band 3446 cm^{-1} is correspond to H-bond [44]. The bands at 1570 cm^{-1} and 1417–1456 cm^{-1} correspond to N–H bond of primary and secondary amides and –C–N- stretching vibration of amides or –C–O– stretching of alcohols, ether, carboxylic acids and anhydrides [45]. The peaks at 901 cm^{-1} and 680 cm^{-1} indicate the presence of alkyl halide groups. The broad absorption peak at 475 cm^{-1} indicates the presence of alcoholic groups. *Eucalyptus globulus* Leaf extract contain simple phenolics and their derivatives, flavonoids and more complex polyphenolic compounds such as proanthocyanidins [46]. These compounds may be responsible for the reduction of metal or metal oxide ion into and formation of nanoparticles [47].

3.2 Characterization of ZnO NPs

In this study, numerous techniques were utilized to describe the structure, morphology, optical, and thermal, properties of ZnO NPs.

3.2.1 UV–Vis analysis

UV–Vis spectroscopy (Fig. 7) revealed a peak at 375 nm, which was typical of ZnO NPs. This was owing to the surface plasmon resonance (SPR), and the sharpened peak confirmed the construction of mono-dispersed ZnO NPs [48]. As a rule of thumb, the absorption peak maximum for ZnO NPs ranges between 300 and 380 nm [49]. The assessed value is lower than that of bulk ZnO given as 380 nm [50] and display a blue shift in excitonic-absorption which specifies a tiny quantum confinement consequence [51].

The straightforward band-gap energy (E_g) for the ZnO NPs is characterized through fitting the reflection data to the straight transform formula $\alpha hv = A\left(hv - E_g\right)^n$, where α is the optical-absorption parameter, hv is the

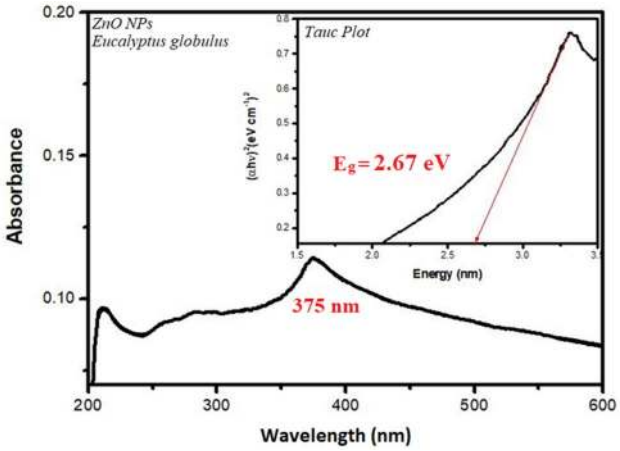

Fig. 7 UV–Vis spectrum of ZnO nanoparticles prepared by *Eucalyptus globulus* leaf extract and zinc nitrate hexahydrate salt, inset: Tauc plot of the same UV–Vis spectrum

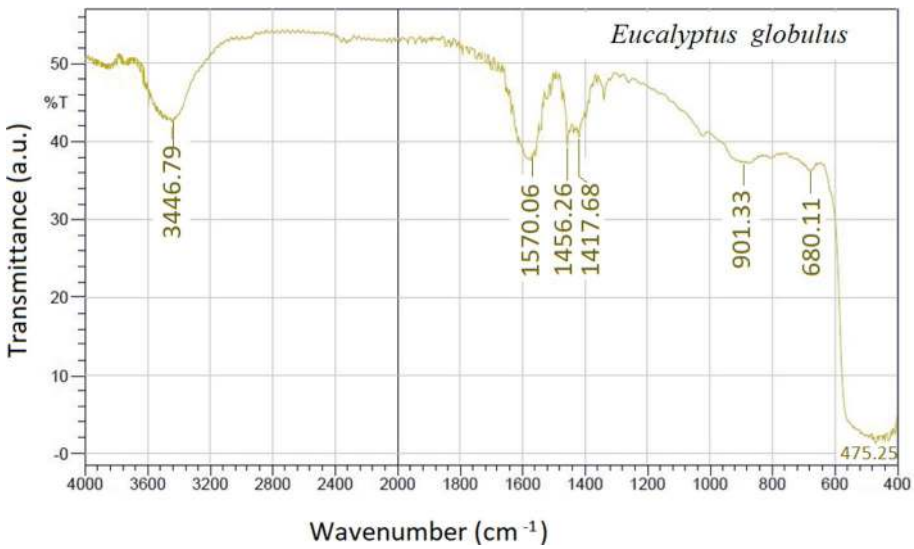

Fig. 6 FTIR spectra of *Eucalyptus globulus* leaf extract

energy of photon, E_g is the straight band-gap, A is a constant and the power n is influenced by the type of optical-transition that predominates. Precisely, with $n = 1/2$, an optimum straightness has been perceived for the straight permitted transition, the best choice in the method considered here. The specific amount of the band-gap is described through the extrapolation of the rectilinear part of $(ahv)^2$ versus hv to the x-axis. The straight band-gap is equals to 2.67 eV for ZnO NPs which is shown in Fig. 7. A decrease in the band-gap is expected as a result of using plant extract, since some plant extract component covers/modifies the surface and reduce the band-gap of the nanoparticles [52]. This consequence does not conflict with the quantum confinement effects especially for the green synthesized nanoparticles. In general, the biosynthesized nanoparticles are more reactive than the equivalent nanoparticles prepared from the other methods [53]. Therefore, the overall high reactivity of particles in the quantum regime can also be attributed to increase in electron populations at the lower energy bands, due to decreased separation of energy states [54]. Metal NPs possess sizes which are much smaller than the wavelength of visible light. They make interaction with light and they can absorb or scatter light. Metal oxides in their bulk status possess a wide band-gap and fewer ability to interact [55] but once their dimensions are decreased, they become supplementary responsive and their aptitude to interact can be inferred from their reflectivity and absorbance capabilities. The absorption peak for ~ 40 nm ZnO NPs has been described by Singh et al. [56] at 361 nm (3.44 eV) and 3.44 eV for the chemical synthesis of ZnO NPs [57], respectively.

3.2.2 FTIR spectroscopy analysis

The FTIR spectrum (Fig. 8), utilized to inspect the pureness and composition of biosynthesized ZnO NPs, reveals no distinct peak in the monitoring range intimating pureness of the ZnO nanoparticles produced by the green process. The broad band at 667 cm^{-1} vanished in the synthesized ZnO nanoparticles. Another peak was formed at 455 cm^{-1} as a result of the formation of ZnO nanoparticles, precisely zinc and oxygen bonding vibrations [58, 59]. The band at 1363 cm^{-1} correlated to the C–O stretching of the carboxylic acid group. While the band found at 1483 cm^{-1}, most probably, related to the –C=C– stretching of the aromatic compounds [60]. The robust and relatively wide band at 3430 cm^{-1} could be allocated to the O–H stretching of phenolic compounds [61].

3.2.3 XRD analysis

X-ray diffraction analysis (Fig. 9) revealed the 2θ characteristic peaks of ZnO at 31.60°, 34.22°, 36.11°, 47.35°, 56.45°, 62.69°, 66.11°, 67.84°, 68.87°, 71.70° and 76.64° for (100), (002), (101), (102), (110), (103), (200), (112), (201), (004) and (202) planes of the crystal lattice, correspondingly. These peaks were agreeable with the regular JCPDS Card No. 89-0510 and proposed the existence of hexagonal Wurtzite form of ZnO NPs. The narrow and robust diffraction peaks point toward the optimum crystalline structure of ZnO NPs. The average crystallite sizes of ZnO NPs were calculated using Debye–Scherrer's equation, i.e. $D = k\lambda/\beta \cos\theta$, where D is crystal size, λ is the wavelength of the X-ray radiation ($\lambda = 0.15406$ nm) for Cu K_α, k is shape factor typically taken as 0.89, β is the full width at high maximum (FWHM) and θ is the diffraction angle [62].

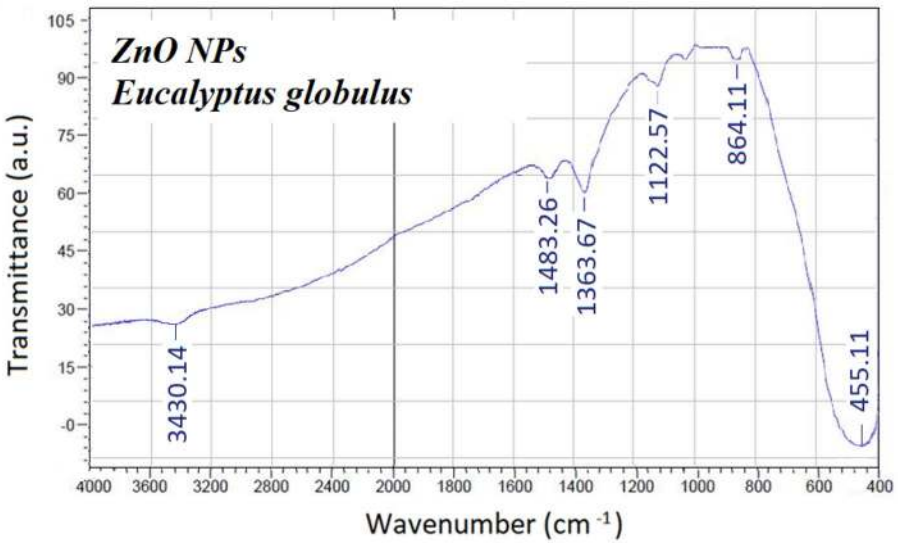

Fig. 8 FTIR spectra of biosynthesized ZnO nanoparticles

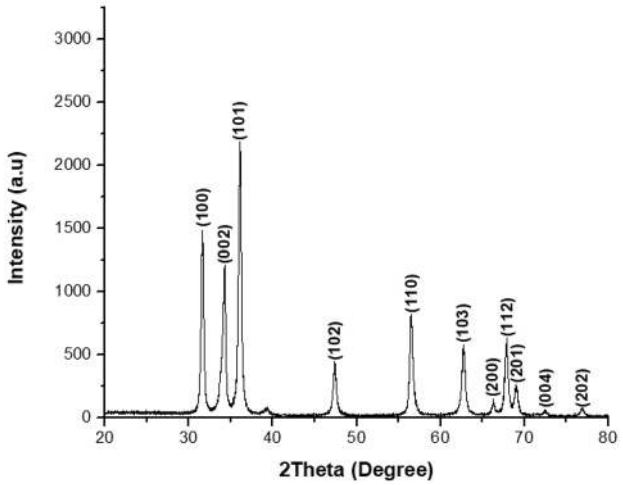

Fig. 9 XRD patterns of ZnO NPs prepared by the biosynthesis method

Table 1 The ZnO NPs particle size calculation using Debye–Scherrer's equation and data from Fig. 9

No. of peaks	Planes	Pos. (°2Th.)	FWHM (°2Th.)	Size (nm)
1	100	31.6341	0.2755	28.97068
2	002	34.2867	0.2558	32.50064
3	101	36.0837	0.2362	35.37301
4	102	47.4023	0.3542	23.49485
5	110	56.46	0.3149	28.63379
6	103	62.753	0.3542	26.27051
7	200	66.2729	0.3149	30.12759
8	112	67.8717	0.2362	40.53903
9	201	69.1166	0.3936	24.50814
10	004	72.3986	0.9446	10.422
11	202	76.8586	0.3936	25.76498
			Average size	27.05502

According to Debye–Scherrer's equation the average crystallite size for ZnO NPs was 27 nm confirmed the nano-size of the ZnO NPs (Table 1). Similar outcomes were found for the biosynthesized ZnO NPs utilizing *Peltophorum pterocarpum* leaf extract [63], *Adhatoda vasica* leaf extract [49] and *Arabic gum* [64].

X-ray diffraction analysis confirmed the existence of even tinier nanoparticles than the SEM inspection. The larger ZnO nanoparticles in the sample caused by the agglomeration of smaller nanoparticles, whose existence is indicated by X-ray diffraction. The X-ray diffraction method allowed for the identifying smaller dimensions of nanoparticles.

The crystallinity of the biosynthesized ZnO NPs also calculated through the following equation [65]:

$$Crystallinity = \frac{Area\ of\ Crystalline\ Peaks}{Area\ of\ all\ Peaks(Crystalline + Amorphous)} \times 100$$

and the crystallinity was, 99.49%.

It can be noted, from the above calculation, that, the crystallinity of the biosynthesized ZnO NPs prepared by both *Eucalyptus globulus* leaf extract and zinc nitrate hexahydrate salt is excellent and very close to 100%. This is very promising results and it was expected since plant extract replaced with the toxic chemicals and the available phytochemicals in the plant extracts participated to produce narrow peaks in XRD spectra and confirmed the crystallinity of synthesized ZnO nanoparticles [66].

3.2.4 SEM analysis

The surface morphology of the biosynthesized ZnO NPs was principally characterized using FESEM analysis and the resulting images are displayed in Fig. 10a. It can be noticed that most of the ZnO NPs are in nanometer scale and are vastly hexagonal in shape with the average diameter of 35 nm. Remarkably, the greatest amount of the ZnO NPs are identical in dimension together with an insufficient large particles. In addition, the ZnO NPs are slightly agglomerated which is typical with the green synthesis nanoparticles. This is due to the fact that biosynthesis NPs possess higher surface area and the durable affinity amongst them cause aggregation or agglomeration [67]. It can be stated that, the ecological factors highly influence the stability of NPs and agglomeration. Thus, throughout the process of nanoparticles formation the NPs stick to each other and impulsively form asymmetrical clusters [68].

Production procedure of ZnO NPs relies upon several growth parameters, comprising concentration of plant extract or biomass, concentration of salt, growth or reaction time, temperature and pH of the solution. Therefore, calibration of these growth elements is essential in gaining the required size and shape of NPs for their maximum manipulation and request.

3.2.5 EDX analysis

In order to expand supplementary vision into the topographies of ZnO NPs, the exploration of the sample was investigated by means of energy dispersive X-ray (EDX) analysis. The EDX spectra of the samples taken from the SEM investigation displaying that the sample produced through the above method has clean ZnO phase [69]. The EDX analysis (Fig. 10b) of the ZnO NPs indicates that our sample contains zinc, oxygen, and gold as essential elements. The EDX spectra displayed two robust peaks for zinc around 1 keV and 8.7 keV, correspondingly and a

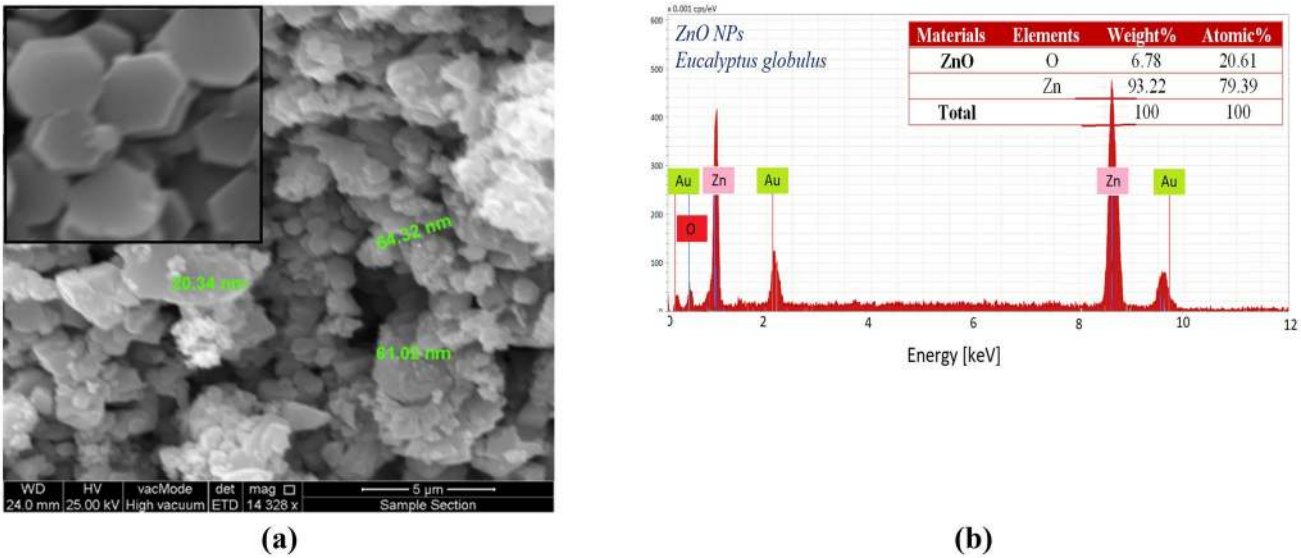

Fig. 10 **a** FESEM and **b** EDX profile of ZnO NPs synthesized from *Eucalyptus globulus* leaf extract

singular peak for oxygen at ~ 0.5 keV, which are typical for ZnO NPs [70]. The presence of gold is as a result of the sample coating throughout FESEM imaging. The high-intensity of zinc and oxygen peaks show that the sample is mostly ZnO. Figure 10b indicated that the ZnO NPs samples possess 93.22% zinc weight percent associated with only 6.78% oxygen weight percent. On the other hand, The atomic percent of zinc was 79.39% accompanying with the 20.61% for oxygen atomic percent which gives the 4:1 ratio for Zn and O, correspondingly.

3.2.6 Dynamic light scattering (DLS) and zeta potential analysis

Debye–Scherrer's equation, which has been mentioned previously, is an approximate conviction which is suitable only for spherical and semispherical particles. Thus, in order to obtain a trustable size measurement of NPs regardless the size and the shapes, one should either use Dynamic Light Scattering (DLS) or transmission electron microscope (TEM). In this study, the average size of the particles and size distribution of biosynthesized ZnO NPs were determined through DLS method. It can be seen, from Fig. 11, that the particle size of ZnO NPs, in general, bigger than the crystallite size in Table 1. Similar combination using chemical method has also reported by Getie et al. [71] and Mayekar et al. [72]. These groups of researchers highlighted that zinc nitrate hexahydrate salt produces smaller ZnO NPs than zinc acetate dehydrate salt.

According to Stokes–Einstein relation the diffusion coefficients can be converted to a hydrodynamic radius as: $D = \frac{k_B T}{6\pi\eta R_h}$, where k_B is Boltzmann's constant, T the temperature, η the viscosity of the suspension medium and R_h the hydrodynamic radius [73]. It can be stated that, compared to XRD, DLS is relatively rapid and inexpensive

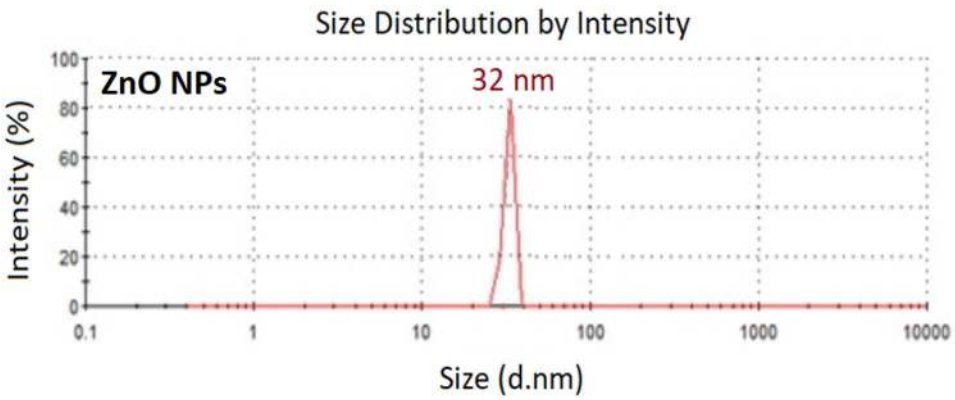

Fig. 11 Particle size distribution using DLS for biosynthesized ZnO NPs

technique to measure a high number of samples. Also, DLS provides considerably larger values, which is perhaps because of the hydrodynamical shell. The size of hydrodynamical shell, in turn, most probably dependent not only on the structure, but also on the shape and roughness of the particle [74].

Zeta potential investigation was performed to identify surface charge and steadiness of biosynthesized ZnO NPs. This study indicated that the capping molecules present on the surface of the biosynthesized ZnO NPs are mainly comprised of negatively charged groups and also responsible for the moderate stability of the nanoparticles. Assessment of zeta potential relies upon the motion of NPs under the impact of an applied electric field. This motion relies on surface charge and the local surroundings of the NPs.

The zeta potential of the biosynthesized ZnO NPs was measured in water as dispersion medium. The average zeta potential value recorded in this investigation was −40 mV (Fig. 12) indicated that the surfaces of biosynthesized ZnO NPs are coated with molecules which are mostly involved of negatively charged groups and likewise in charge for steadiness of the nanoparticles [75]. Similar results have been found by Azizi et al. [75]. It can be understood that, if the value of zeta potential between 0 to ± 5, ± 10 to ± 30, ± 30 to ± 40, ± 40 to ± 60 and > ±61 mV is an indicator for rapid coagulation, incipient instability, moderate stability, good stability, and excellent stability respectively [76]. Thus, our biosynthesized ZnO NPs possess good stability. This result is a good indicator that these nanoparticles possess considerable active adsorption sites to absorb dyes, and heavy metal ions from aqueous systems.

3.2.7 DSC analysis

Differential scanning calorimetry (DSC) can validate an alteration in melting temperatures depending on grain size. Generally, the melting temperature of nanoparticles can be − 263.15 to − 173.15 °C beneath the bulk material due to a greater value of surface/volume ratio [77]. DSC analysis was utilized to describe the decomposition and thermal stability of nanoparticles measured from 50 to 600 °C at the heating rate of 10 °C/min. It can be seen, from Fig. 12, that the DSC curve of the biosynthesized ZnO NPs exhibits two endothermic peaks with one exothermic peak centered at about 111.35, 223, 271.95 °C and 365.11 respectively. A tiny endothermic peak recorded near 111.35 °C, initiated at 100 °C is assigned to the vaporization of the absorbed water by ZnO NPs. This tiny displacement from 100 to 111.35 °C might be ascribed to the loss of unstable wetting agent molecules adsorbed on the surface of ZnO NPs throughout synthesizing process [78]. While, the exothermic peak that appeared at 365.11 °C is, perhaps, owing to the formation of ZnO NPs and degradation of organic materials. This is a good indicator that, despite the crystallinity of the ZnO NPs which has been verified by XRD analysis (Fig. 9), the ZnO NPs need further annealing until around 365 °C in order to be more purified. Lastly, the peak nearby 271.95 °C is, most likely, allocated to the alteration of zinc complex to zinc hydroxide ($Zn(OH)_2$) [79].

3.2.8 Thermal stability

The thermogravimetric analysis (TGA) have been conducted on the biosynthesized ZnO NPs. Figure 13 illustrates that the 2.3% weight-loss initiates lightly at 114 °C

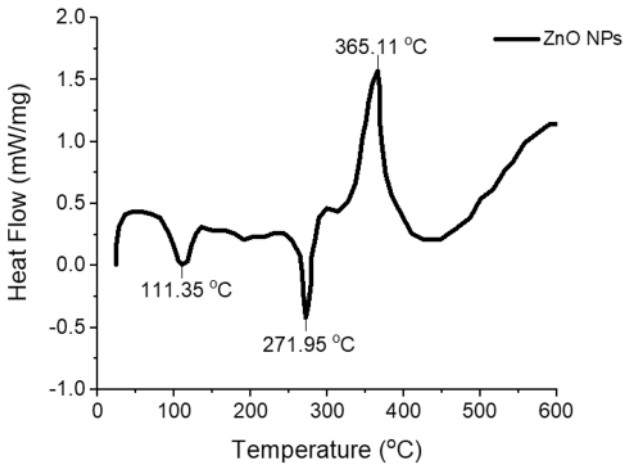

Fig. 12 Differential scanning calorimetry curve of the biosynthesized ZnO NPs

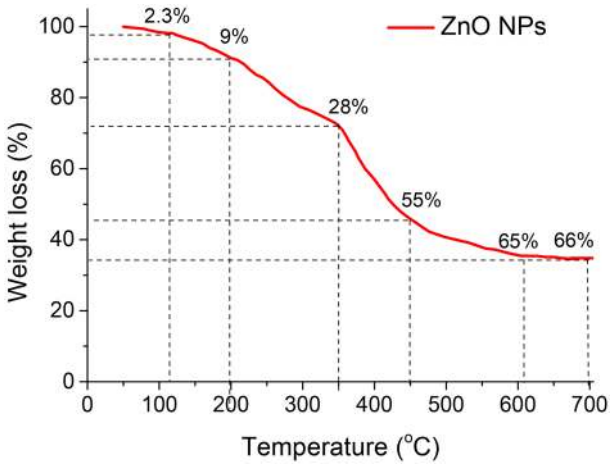

Fig. 13 Thermogravimetric analysis (TGA) of the biosynthesized ZnO NPs

followed by the 9% weight-loss at 200 °C due to the evaporation of water. The considerable weight-loss happened amongst 350 and 600 °C, which was about 65% of the actual weight as a result of the elimination and breakdown of organic-groups existing in the specimen throughout the biosynthesis process. Above 700 °C there was not any significant breakdown or reaction. The exothermic peak observed in the DSC curve (Fig. 12) shows the highest peak at 365.11 °C which is, more likely, correspond to 28% weight-loss as a result of burning out the organic compound.

3.2.9 BET surface area analysis

The BET analysis objectives to offer a description for the physical-adsorption of gas molecules on a solid surface and works as the origin for a crucial investigation method to directly measures surface area and pore size distribution. In 1938, Brunauer, Emmett, and Teller published the leading article about the BET analysis in the journal of the American Chemical Society [80]. The BET principle denotes to multilayer adsorption and normally accepts noncorrosive gases, i.e. nitrogen, argon and carbon dioxide, in our case we utilized nitrogen gas as adsorbates to find the surface area of ZnO NPs [81].

To find the surface area of ZnO NPs, BET equation [80], $\frac{1}{W\left(\left(\frac{P_o}{P}\right)-1\right)} = \frac{1}{W_m C} + \frac{C-1}{W_m C}\left(\frac{P}{P_o}\right)$ has been utilized. Where W is the weight of gas adsorbed, P/Po is the relative pressure, Wm is the weight of adsorbate as monolayer and C is the BET constant. BET equation needs a linear plot (Fig. 14) of $\frac{1}{W\left(\left(\frac{P_o}{P}\right)-1\right)}$ contrary to $\frac{P}{P_o}$.

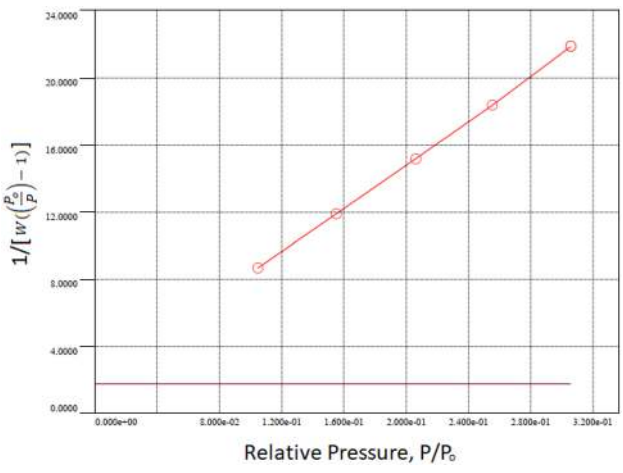

Fig. 14 Linear plot of BET equation to determine surface area of ZnO NPs

In BET equation $s = \frac{C-1}{W_m C} = 65.409$ represents the slope of the line in Fig. 13. While $i = \frac{1}{W_m C} = 1.758$ represents the intercept of the line. After careful combinations between both the slope and the intercept one can easily find the weight of monolayer $W_m = \frac{1}{S+i} = 0.01488$. Then total surface area S_t can be calculated from $S_t = \frac{W_m N_a A_{cs}}{M}$, where N_a is Avogadro's number, $6.02214 \times 10^{23}\ \text{mol}^{-1}$, M is the molecular weight of Adsorbate, $M_{ZnO} = 81.38$ g/mol, and A_{sc} is Adsorbate cross sectional area $A_{cs} = 16.200\ \text{Å}^2$ for Nitrogen. Then specific surface area S can be calculated by $S = S_t/w$, where w is the utilized sample weight, 0.760 g. The specific surface area S of the ZnO powder was 23.481 m^2/g, which corresponds to a Hexagonal particle size of 32 nm from *Eucalyptus globulus* plant extract and zinc nitrate hexahydrate salt. Similar result has been found by Tarafdar et al. [82] using spherical ZnO nanoparticles with particles sizes ranging between 16 and 30 nm. The effect of surface area for developing photocatalytic behavior is very important because of its aptitude to enable many active places to adsorb organic pollutants on the surface of catalyst, i.e. ZnO NPs in our case. The larger surface area might offer the adsorption of organic pollutants on the surface of the catalyst, possibly will result in improving photocatalytic activity. Thus, the biosynthesized ZnO NPs are predicted to display superior photocatalytic activity which can be used for water purification.

4 Conclusions

Biosynthesis of ZnO NPs with the use of plant extract has improved remarkably due to their heterogeneous requests. This study involved, a quick and economic biosynthesis of ZnO NPs from aqueous leaf extract *Eucalyptus globulus* and zinc nitrate hexahydrate salt. The effective ingredients existent in *Eucalyptus globulus* leaf extract are behaving as a reducing agent along with the capping and stabilizing agents for the production of ZnO nanoparticles.

Several techniques, namely UV–Vis spectroscopy, FTIR analysis, XRD, SEM, EDX, BET, DLS and DSC have been utilized in this investigation to analyze both the property and quality of the biosynthesized ZnO NPs. These techniques showed that the property of the biosynthesized ZnO NPs is comparable with the standard NPs prepared from different methods. Moreover, this study showed that *Eucalyptus globulus* leaf extract is a good candidate for biosynthesizing ZnO NPs due the existence of the vital phytochemicals that can act as a platform, in this manner playing the role of reducing in addition to capping agents in the biosynthesizing of nanoparticles.

The utilized green method, in this investigation, provides hexagonal ZnO NPs with average diameter of 35 nm

and very high crystallinity. Also, there was an excellent agreement between the particle size measurement using different methods. DSC analysis indicated that, despite the very high crystallinity of the ZnO NPs, the ZnO NPs require additional annealing till about 365 °C in order to be more purified. The biosynthesized ZnO NPs are thermally stable and until 350 °C there was not any considerable weight-loss. The specific surface area of the biosynthesized ZnO NPs was 23.481 m^2/g, which means each gram of the biosynthesized ZnO NPs is sufficient to cover a 6×4 m^2 room. This study showed that through this green and economical method, high quality, thermally stable and nanosize ZnO particle can be produced in industrial scale and later can be utilized in diverse applications. According to zeta potential analysis the biosynthesized ZnO NPs in this study possess good stability. This result is a good indicator that these nanoparticles possess considerable active adsorption sites to absorb dyes, and heavy metal ions from aqueous systems. Finally, due to the continuous exertions to expand and enhance the aptitude of metallic and metal oxide NPs synthesis, the green synthesis method is expected to expand the application of ZnO NPs in medication and cultivation in the coming years.

Acknowledgements Himdad Hamad Azeez is thankful to Salahaddin University-Erbil, Iraq, for being an MSc. student and fully supported by them. The authors would like to thank Soran research center for providing all the facilities to perform the research work. In addition, the authors thank Dr Mukhtar Ahmed at SISAF, Ulster University, UK, Garmian University and Koya University for their valuable assistance throughout this investigation. Finally, a sincere thank goes to Dr David M.W. Waswa at Tishk International University for his diligent proofreading of this manuscript.

Compliance with ethical standards

Conflict of interest The author(s) declare that they have no competing interests.

References

1. Boisseau P, Loubaton B (2011) Nanomedicine, nanotechnology in medicine. C R Phys 12:620–636
2. Suri SS, Fenniri H, Singh B (2007) Nanotechnology-based drug delivery systems. J Occup Med Toxicol 2:16
3. Bhattacharya S, Saha I, Mukhopadhyay A, Chattopadhyay D, Chand U (2013) Role of nanotechnology in water treatment and purification: potential applications and implications. Int J Chem Sci Technol 3:59–64
4. Rai M, Ingle A (2012) Role of nanotechnology in agriculture with special reference to management of insect pests. Appl Microbiol Biotechnol 94:287–293
5. Duncan TV (2011) Applications of nanotechnology in food packaging and food safety: barrier materials, antimicrobials and sensors. J Colloid Interface Sci 363:1–24
6. Stelzner T, Pietsch M, Andrä G, Falk F, Ose E, Christiansen S (2008) Silicon nanowire-based solar cells. Nanotechnology 19:295203
7. Raj S, Jose S, Sumod U, Sabitha M (2012) Nanotechnology in cosmetics: opportunities and challenges. J Pharm Bioallied Sci 4:186
8. Wong Y, Yuen C, Leung M, Ku S, Lam H (2006) Selected applications of nanotechnology in textiles. Autex Res J 6:1–8
9. De Franceschi S, Kouwenhoven L (2002) Nanotechnology: electronics and the single atom. Nature 417:701
10. Liu H-L, Dai SA, Fu K-Y, Hsu S-H (2010) Antibacterial properties of silver nanoparticles in three different sizes and their nanocomposites with a new waterborne polyurethane. Int J Nanomed 5:1017
11. Krutyakov YA, Kudrinskiy AA, Olenin AY, Lisichkin GV (2008) Synthesis and properties of silver nanoparticles: advances and prospects. Russ Chem Rev 77:233
12. Geethalakshmi R, Sarada D (2013) Characterization and antimicrobial activity of gold and silver nanoparticles synthesized using saponin isolated from *Trianthema decandra* L. Ind Crop Prod 51:107–115
13. Aiad I, El-Sukkary MM, Soliman E, El-Awady MY, Shaban SM (2014) In situ and green synthesis of silver nanoparticles and their biological activity. J Ind Eng Chem 20:3430–3439
14. Stevanović MM, Škapin SD, Bračko I, Milenković M, Petković J, Filipič M, Uskoković DP (2012) Poly(lactide-co-glycolide)/silver nanoparticles: synthesis, characterization, antimicrobial activity, cytotoxicity assessment and ROS-inducing potential. Polymer 53:2818–2828
15. Wahab R, Mishra A, Yun S-I, Kim Y-S, Shin H-S (2010) Antibacterial activity of ZnO nanoparticles prepared via non-hydrolytic solution route. Appl Microbiol Biot 87:1917–1925
16. Premanathan M, Karthikeyan K, Jeyasubramanian K, Manivannan G (2011) Selective toxicity of ZnO nanoparticles toward Gram-positive bacteria and cancer cells by apoptosis through lipid peroxidation. Nanomedicine NBM 7:184–192
17. Lee YS, Kim DW, Lee YH, Oh JH, Yoon S, Choi MS, Lee SK, Kim JW, Lee K, Song C-W (2011) Silver nanoparticles induce apoptosis and G2/M arrest via PKCζ-dependent signaling in A549 lung cells. Arch Toxicol 85:1529–1540
18. Arabi M, Ghaedi M, Ostovan A (2017) Development of a lower toxic approach based on green synthesis of water-compatible molecularly imprinted nanoparticles for the extraction of hydrochlorothiazide from human urine. ACS Sustain Chem Eng 5:3775–3785
19. Liu J, Qiao SZ, Hu QH, Lu GQ (2011) Magnetic nanocomposites with mesoporous structures: synthesis and applications. Small 7:425–443
20. Mohanpuria P, Rana NK, Yadav SK (2008) Biosynthesis of nanoparticles: technological concepts and future applications. J Nanopart Res 10:507–517
21. Marshall AT, Haverkamp RG, Davies CE, Parsons JG, Gardea-Torresdey JL, van Agterveld D (2007) Accumulation of gold nanoparticles in *Brassic juncea*. Int J Phytoremediat 9:197–206
22. Kim J, Rheem Y, Yoo B, Chong Y, Bozhilov KN, Kim D, Sadowsky MJ, Hur H-G, Myung NV (2010) Peptide-mediated shape-and size-tunable synthesis of gold nanostructures. Acta Biomater 6:2681–2689
23. Malik P, Shankar R, Malik V, Sharma N, Mukherjee TK (2014) Green chemistry based benign routes for nanoparticle synthesis. J Nanopart 2014:1–14
24. Dwivedi AD, Gopal K (2010) Biosynthesis of silver and gold nanoparticles using *Chenopodium album* leaf extract. Colloid Surf A 369:27–33
25. Mittal AK, Chisti Y, Banerjee UC (2013) Synthesis of metallic nanoparticles using plant extracts. Biotechnol Adv 31:346–356

26. Djurišić AB, Leung YH, Ng AMC (2014) Strategies for improving the efficiency of semiconductor metal oxide photocatalysis. Mater Horiz 1:400–410
27. Król A, Pomastowski P, Rafińska K, Railean-Plugaru V, Buszewski B (2017) Zinc oxide nanoparticles: synthesis, antiseptic activity and toxicity mechanism. Adv Colloid Interface 249:37–52
28. Wang ZL, Song J (2006) Piezoelectric nanogenerators based on zinc oxide nanowire arrays. Science 312:242–246
29. Xia T, Kovochich M, Liong M, Madler L, Gilbert B, Shi H, Yeh JI, Zink JI, Nel AE (2008) Comparison of the mechanism of toxicity of zinc oxide and cerium oxide nanoparticles based on dissolution and oxidative stress properties. ACS Nano 2:2121–2134
30. Qi K, Cheng B, Yu J, Ho W (2017) Review on the improvement of the photocatalytic and antibacterial activities of ZnO. J Alloys Compd 727:792–820
31. Islam MT, Dominguez A, Alvarado-Tenorio B, Bernal RA, Montes MO, Noveron JC (2019) Sucrose-mediated fast synthesis of zinc oxide nanoparticles for the photocatalytic degradation of organic pollutants in water. ACS Omega 4:6560–6572
32. Serpone N, Emeline A (2012) Semiconductor photocatalysis: past, present, and future outlook. ACS Publications, New York
33. Hardel DK, Laxmidhar S (2011) A review on phytochemical and pharmacological of *Eucalyptus globulus*: a multipurpose tree. Int J Res Ayurveda Pharm 2:1527–1530
34. Sathishkumar M, Sneha K, Yun Y-S (2010) Immobilization of silver nanoparticles synthesized using *Curcuma longa tuber* powder and extract on cotton cloth for bactericidal activity. Bioresour Technol 101:7958–7965
35. Singh P, Kim YJ, Zhang D, Yang DC (2016) Biological synthesis of nanoparticles from plants and microorganisms. Trends Biotechnol 34:588–599
36. Hocine R, Mazauric J, Madani K, Boulekbache-Makhlouf L (2016) Phytochemical analysis and antioxidant activity of *Eucalyptus globulus*: a comparative study between fruits and leaves extracts. J Chem Eng Bio Chem 1:23–29
37. Ovais M, Khalil AT, Raza A, Khan MA, Ahmad I, Islam NU, Saravanan M, Ubaid MF, Ali M, Shinwari ZK (2016) Green synthesis of silver nanoparticles via plant extracts: beginning a new era in cancer theranostics. Nanomedicine 12:3157–3177
38. Wang M, Zhou Y, Zhang Y, Hahn SH, Kim EJ (2011) From $Zn(OH)_2$ to ZnO: a study on the mechanism of phase transformation. Cryst Eng Comm 13:6024–6026
39. Pretsch E, Bühlmann P, Affolter C, Pretsch E, Bhuhlmann P, Affolter C (2000) Structure determination of organic compounds. Springer, Berlin, p 108
40. Makarov V, Love A, Sinitsyna O, Makarova S, Yaminsky I, Taliansky M, Kalinina N (2014) "Green" nanotechnologies: synthesis of metal nanoparticles using plants. Acta Nat 6:35–44
41. Faizi S, Siddiqi H, Naz A, Bano S (2010) Specific deuteration in patuletin and related flavonoids via keto-enol tautomerism: solvent-and temperature-dependent 1H-NMR studies. Helv Chim Acta 93:466–481
42. Rasheed T, Nabeel F, Bilal M, Iqbal HM (2019) Biogenic synthesis and characterization of cobalt oxide nanoparticles for catalytic reduction of direct yellow-142 and methyl orange dyes. Biocatal Agric Biotechnol 19:101154
43. Khalafi T, Buazar F, Ghanemi K (2019) Phycosynthesis and enhanced photocatalytic activity of zinc oxide nanoparticles toward organosulfur pollutants. Sci Rep 9:6866
44. Sharmila G, Muthukumaran C, Sandiya K, Santhiya S, Pradeep RS, Kumar NM, Suriyanarayanan N, Thirumarimurugan M (2018) Biosynthesis, characterization, and antibacterial activity of zinc oxide nanoparticles derived from *Bauhinia tomentosa* leaf extract. J Nanostruct Chem 8:293–299
45. Ishnava KB, Chauhan JB, Barad MB (2013) Anticariogenic and phytochemical evaluation of *Eucalyptus globules* Labill. Saudi J Biol Sci 20:69–74
46. Parveen A, Roy AS, Rao S (2012) Biosynthesis and characterization of silver nanoparticles from *Cassia auriculata* leaf extract and in vitro evaluation of antimicrobial activity. Int J Appl Biol Pharm 3:222–228
47. Kim JP, Lee IK, Yun BS, Chung SH, Shim GS, Koshino H, Yoo ID (2001) Ellagic acid rhamnosides from the stem bark of *Eucalyptus globulus*. Phytochemistry 57:587–591
48. Santos SA, Carmen SF, Rosário M, Domingues M, Armando JD, Carlos PN (2011) Characterization of phenolic components in polar extracts of *Eucalyptus globulus* Labill. bark by high-performance liquid chromatography–mass spectrometry. J Agric Food Chem 59:9386–9393
49. Pai S, Sridevi H, Varadavenkatesan T, Vinayagam R, Selvaraj R (2019) Photocatalytic zinc oxide nanoparticles synthesis using *Peltophorum pterocarpum* leaf extract and their characterization. Optik 185:248–255
50. Varadavenkatesan T, Lyubchik E, Pai S, Pugazhendhi A, Vinayagam R, Selvaraj R (2019) Photocatalytic degradation of Rhodamine B by zinc oxide nanoparticles synthesized using the leaf extract of *Cyanometra ramiflora*. J Photochem Photobiol B 199:111621
51. Qin L, Shing C, Sawyer S, Dutta PS (2011) Enhanced ultraviolet sensitivity of zinc oxide nanoparticle photoconductors by surface passivation. Opt Mater 33:359–362
52. Koch U, Fojtik A, Weller H, Henglein A (1985) Photochemistry of semiconductor colloids. Preparation of extremely small ZnO particles, fluorescence phenomena and size quantization effects. Chem Phys Lett 122:507–510
53. Khan MM, Saadah NH, Khan ME, Harunsani MH, Tan AL, Cho MH (2019) Potentials of *Costus woodsonii* leaf extract in producing narrow band gap ZnO nanoparticles. Mater Sci Semicond Process 91:194–200
54. Pantidos N, Horsfall LE (2014) Biological synthesis of metallic nanoparticles by bacteria, fungi and plants. J Nanomed Nanotechnol 5:1
55. Jiang J, Oberdörster G, Elder A, Gelein R, Mercer P, Biswas P (2008) Does nanoparticle activity depend upon size and crystal phase? Nanotoxicology 2:33–42
56. Rodriguez JA, Wang X, Hanson JC, Liu G, Iglesias-Juez A, Fernández-García M (2003) The behavior of mixed-metal oxides: structural and electronic properties of Ce_{1-x} Ca_x O_2 and Ce_{1-x} Ca_x O_{2-x}. J Chem Phys 119:5659–5669
57. Singh D, Singh J, Mishra P, Tiwari R, Srivastava O (2008) Synthesis, characterization and application of semiconducting oxide (Cu_2O and ZnO) nanostructures. B Mater Sci 31:319–325
58. Balcha A, Yadav OP, Dey T (2016) Photocatalytic degradation of methylene blue dye by zinc oxide nanoparticles obtained from precipitation and sol–gel methods. Environ Sci Pollut Res 23:25485–25493
59. Yuvakkumar R, Suresh J, Saravanakumar B, Nathanael AJ, Hong SI, Rajendran V (2015) Rambutan peels promoted biomimetic synthesis of bioinspired zinc oxide nanochains for biomedical applications. Spectrochim Acta A Mol Biomol Spectrosc 137:250–258
60. Bhuyan T, Mishra K, Khanuja M, Prasad R, Varma A (2015) Biosynthesis of zinc oxide nanoparticles from *Azadirachta indica* for antibacterial and photocatalytic applications. Mater Sci Semicond Process 32:55–61
61. Hu D, Si W, Qin W, Jiao J, Li X, Gu X, Hao Y (2019) Cucurbita pepo leaf extract induced synthesis of zinc oxide nanoparticles, characterization for the treatment of femoral fracture. J Photochem Photobiol B 195:12–16

62. Ganesh M, Lee SG, Jayaprakash J, Mohankumar M, Jang HT (2019) *Hydnocarpus alpina* Wt extract mediated green synthesis of ZnO nanoparticle and screening of its anti-microbial, free radical scavenging, and photocatalytic activity. Biocatal Agric Biotechnol 19:101129
63. Vijayalakshmi R, Rajendran V (2012) Synthesis and characterization of nano-TiO_2 via different methods. Arch Appl Sci Res 4:1183–1190
64. Sonia S, Ruckmani K, Sivakumar M (2017) Antimicrobial and antioxidant potentials of biosynthesized colloidal zinc oxide nanoparticles for a fortified cold cream formulation: a potent nanocosmeceutical application. Mater Sci Eng C 79:581–589
65. Fardood ST, Ramazani A, Moradi S, Asiabi PA (2017) Green synthesis of zinc oxide nanoparticles using arabic gum and photocatalytic degradation of direct blue 129 dye under visible light. J Mater Sci Mater Electron 28:13596–13601
66. Frost K, Daniel K, Gemma K, Edmond L, Robert S (2009) Crystallinity and structure of starch using wide angle X-ray scattering. Carbohyd Polym 78:543–548
67. Sundrarajan M, Ambika S, Bharathi K (2015) Plant-extract mediated synthesis of ZnO nanoparticles using *Pongamia pinnata* and their activity against pathogenic bacteria. Adv Powder Technol 26:1294–1299
68. Agarwal H, Kumar SV, Rajeshkumar S (2017) A review on green synthesis of zinc oxide nanoparticles—an eco-friendly approach. Resour Eff Technol 3:406–413
69. Vidya C, Hiremath S, Chandraprabha M, Antonyraj ML, Gopal IV, Jain A, Bansal K (2013) Green synthesis of ZnO nanoparticles by *Calotropis gigantea*. Int J Curr Eng Technol 1:118–120
70. Kumar SS, Venkateswarlu P, Rao VR, Rao GN (2013) Synthesis, characterization and optical properties of zinc oxide nanoparticles. Int Nano Lett 3:30
71. Shim YJ, Soshnikova V, Anandapadmanaban G, Mathiyalagan R, Perez ZEJ, Markus J, Kim YJ, Castro-Aceituno V, Yang DC (2019) Zinc oxide nanoparticles synthesized by *Suaeda japonica* Makino and their photocatalytic degradation of methylene blue. Optik 182:1015–1020
72. Getie S, Belay A, Chandra Reddy AR, Belay Z (2017) Synthesis and characterizations of zinc oxide nanoparticles for antibacterial applications. J Nanomedic Nanotechnol 8:2–8
73. Mayekar J, Dhar V, Radha S (2014) Role of salt precursor in the synthesis of zinc oxide nanoparticles. Int J Res Eng Technol 3:43–45
74. Kätzel U, Manuel V, Michael S, Torsten G, Herbert B (2008) Dynamic light scattering for the characterization of polydisperse fractal systems: II. Relation between structure and DLS results. Part Part Syst Charact 25:19–30
75. Azizi S, Mahdavi S, Mohamad MR (2017) Green synthesis of zinc oxide nanoparticles for enhanced adsorption of lead ions from aqueous solutions: equilibrium, kinetic and thermodynamic studies. Molecules 22:831–845
76. Kumar A, Dixit CK (2017) Methods for characterization of nanoparticles. In: Advances in nanomedicine for the delivery of therapeutic nucleic acids. Woodhead Publishing, pp 43–58
77. Aerts A, Lana Follens R, Mohamed H, Tom P, Marc-André D, Benoit L, Jan V (2007) Combined NMR, SAXS, and DLS study of concentrated clear solutions used in silicalite-1 zeolite synthesis. Chem Mater 19:3448–3454
78. Jiang A, Awasthi N, Kolmogorov AN, Setyawan W, Börjesson A, Bolton K, Harutyunyan AR, Curtarolo S (2007) Theoretical study of the thermal behavior of free and alumina-supported Fe–C nanoparticles. Phys Rev B 75:205426
79. Fernandes D, Silva R, Hechenleitner AW, Radovanovic E, Melo MC, Pineda EG (2009) Synthesis and characterization of ZnO, CuO and a mixed Zn and Cu oxide. Mater Chem Phys 115:110–115
80. Kołodziejczak-Radzimska A, Jesionowski T (2014) Zinc oxide-from synthesis to application: a review. Materials 7:2833–2881
81. Brunauer S, Emmett PH, Teller E (1938) Adsorption of gases in multimolecular layers. J Am Chem Soc 60:309–319
82. Ebadi A, Mohammadzadeh JS, Khudiev A (2009) What is the correct form of BET isotherm for modeling liquid phase adsorption? Adsorption 15:65–73